NMR studies of $NbSe_3$: Electronic structures, static charge-density-wave measurements, and observations of the moving charge-density wave

Joseph H. Ross, Jr.,* Zhiyue Wang,† and Charles P. Slichter‡
Department of Physics and Materials Research Laboratory, University of Illinois at Urbana-Champaign, Urbana, Illinois 61801
(Received 7 August 1989)

We describe a series of ^{93}Nb NMR studies of the charge-density-wave (CDW) conductor $NbSe_3$. Using an aligned, multicrystalline sample, we have measured the complete shift tensors for the three Nb sites in the normal state. The results confirm a picture in which one chain is essentially insulating, and the other two are conducting. Studies below the 144-K CDW transition give well-resolved CDW-broadened line shapes, which indicate that the CDW is incommensurate with little or no lock-in to the lattice. Further NMR measurements performed with the CDW driven by electrical currents give information about the moving CDW. Motional narrowing of the NMR line indicates that the CDW conduction phenomena are associated with bulk motion of the $NbSe_3$ CDW. On the other hand, the motion is irregular at all voltages, as indicated by the large voltage required for motional narrowing, the short T_2, and the behavior of the magnetization under current-induced saturation. Furthermore, NMR spin-echo measurements of the low-voltage dielectric response indicate a spatially nonuniform response of the CDW under its pinning barriers.

I. INTRODUCTION

$NBSe_3$ has attracted a great deal of attention since the discovery of mobile incommensurate charge-density waves (CDW's) in the material.[1] The CDW's in $NbSe_3$ can be set into motion by the application of a small electric field, as evidenced by observations of the non-Ohmic conductivity[2] and narrow-band noise.[3]

The $NbSe_3$ unit cell contains three inequivalent types of chains,[4] which form the backbone of the fibrous crystals. The three chains have been labeled "red," "orange," and "yellow" by Wilson,[5] a notation which we will use in this paper. Figure 1 shows the structure projected perpendicular to the chain axis (which is the *b* crystal axis), and in the figure the three Nb sites are labeled according to the Wilson notation.

$NbSe_3$ exhibits two apparently independent CDW's. Both are incommensurate, but have periods of nearly four lattice constants.[6] One CDW is observed at temperatures below 144 K. The second is observed at temperatures below 59 K. Observed in both temperature regimes are conduction phenomena such as the non-Ohmic conductivity and the narrow-band noise. Our studies have concentrated mainly on the higher-temperature CDW, at temperatures above 59 K, although we report some results at lower temperatures.

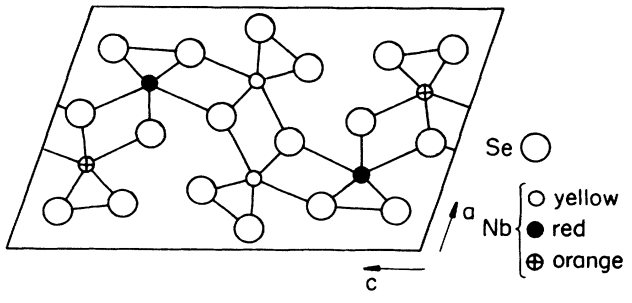

FIG. 1. $NbSe_3$ unit cell, viewed along the *b* axis (long crystal axis). The site labels are those of Ref. 5; structure data from Ref. 14.

We describe a set of ^{93}Nb NMR experiments. In these experiments, aligned multicrystalline samples of $NbSe_3$ have been used for NMR measurements with and without electric current flow in the crystals. The results give information about the characteristics of the Nb sites in the normal state, the structure of the higher-temperature incommensurate CDW, and the motion of the CDW with applied electric fields. A brief account of this work has been reported earlier.[7]

NMR (Refs. 8 and 9) and NQR (Ref. 10) studies of $NbSe_3$ have already appeared. Devreux[8] has observed the broadening of the quadrupolar satellites at the transitions, characteristic of CDW's localized on two of the three structural chains in $NbSe_3$. On the other hand, in the NQR study of Suits and Slichter,[10] large changes in one site were observed below the 144-K transition, but without the expected broadening. We thus undertook the construction of the aligned sample in order to obtain the additional information available from a high-field, single-crystal spectrum.

Sample characteristics are described in Sec. II. As a result of the preparation of an aligned sample, we have been able to resolve the complete Knight shift and electric field-gradient tensors in the normal state (above 144 K). These results will be described in Sec. III. We have also used numerical calculations to analyze the observed

field gradients, and these will be discussed in Sec. III, as well. Below the transitions, we have observed sharp spectra, with a well-resolved effect of the CDW on the line shapes. These results and the analysis will be given in Sec. IV.

For investigation of the NMR under current flow, a second sample was constructed which contains crystals attached to current leads. Using this sample we have observed the current-induced motional narrowing of the CDW-broadened line, and the saturation of the resonance, which indicate bulk motion of the CDW above the conduction threshold. These studies will be described in Sec. V. In addition, NMR with small current pulses allows us to characterize the dielectric displacement of the CDW, as described in Sec. VI.

II. SAMPLES

Samples were prepared from crystals grown in our laboratory. The $NbSe_3$ crystal growth is described by Suits and Slichter,[10] and followed the standard technique.[11] Our crystals can be characterized by the conduction thresholds, typically 100 mV/cm in the higher-temperature CDW regime and 10 mV/cm in the lower-temperature CDW regime, comparable to those of high-quality crystals reported in the literature.

For NMR studies with no current flow, an aligned sample was prepared containing roughly 300 crystals. The crystals are fastened between cover glass slides and adhesive tape, so that they remain electrically isolated from each other, to minimize eddy currents. In the sample the crystals are aligned so that the long crystal axes are all parallel, and the flat facets of the ribbonlike crystals are also parallel. From the NMR spectra we could detect a distribution in the crystal orientations corresponding to twists about the long axis, with a width of roughly 5°. On the other hand, the long axes were much more precisely aligned, and no distribution could be detected in our experiments.

The crystal shape reflects the interchain bonding, which is much stronger along c than perpendicular to c (see Fig. 1). Thus, the flat ribbon facets contain the c axis, while b lies along the long axes of the crystals. By orienting the crystals as described above, the b and c axes were all aligned, but there are two possible orientations for the a axis among the different crystals. Thus, in general, two sets of spectra per site were observed. With the magnetic field oriented in the b-c plane, though, the symmetry is such that the two orientations give equivalent spectra.

For current-flow NMR studies, a $NbSe_3$ sample was constructed containing 30 crystals, from one growth batch. The crystals were mounted on a piece of copper-clad glass-fiber-epoxy printed circuit board, etched to leave two copper lines on opposite edges for electrical contacts. The distance between contacts is 1 cm, and the crystals are connected in parallel.

In the current-flow sample the crystals are aligned only on the long (b) axis, and our studies were confined to the sample orientation with the magnetic field along b, for which the a- and c-axis orientations are irrelevant. This sample contains approximately 3 μg of $NbSe_3$, or 6×10^{16} spins per site. This sample required typically 10^6 spin echoes signal-averaged to produce a reasonable signal in our apparatus, at 77 K and 84 kG, with a repetition rate of 30 ms.

Electrical contacts to the crystals were made using Wood's metal, a low-melting-point solder. The copper was first wetted with Wood's metal, and then individual crystals were attached by melting a small spot of the solder at each end of the crystal. No special surface preparation of the crystals was performed. In this way electrical contacts could be made quite reliably, and the contacts are durable through repeated thermal cycling. Tests of this method using individual crystals showed that contact resistances are typically a few ohms, much smaller than the individual crystal resistances. Furthermore, with individual crystals, we observed sharp conduction thresholds and narrow-band-noise spectra, just as observed with the more common silver paint contacts.

To characterize the current-flow NMR sample, we have observed both its non-Ohmic conductivity and narrow-band-noise spectra. The differential resistivity was measured using a lock-in amplifier. The differential resistivity is characterized not by a single sharp conduction threshold, but by a distribution in thresholds, related presumably to the variations among individual crystals. At 100 K several individual thresholds are observed, in the range 40–100 mV/cm, as shown in Fig. 2. At 77 K

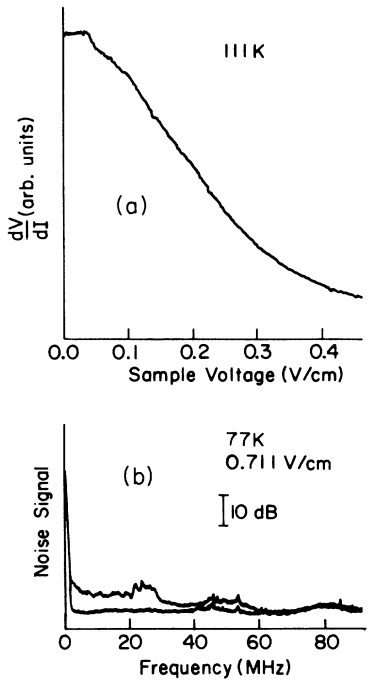

FIG. 2. Electrical characteristics of the sample used for all current-flow NMR studies in this work. (a) Differential resistivity measured at 115 K, illustrating the distribution in conduction thresholds. (b) Narrow-band noise measured at 77 K. The upper trace was obtained with a sample bias of 0.711 V/cm, and the lower trace with no sample bias, indicating background noise. A fundamental at 25 MHz, and its harmonic, are apparent.

the threshold is more rounded, and also at larger voltages, distributed between 100 and 200 mV/cm. Determination of the threshold was aided by the observation of the voltage at which the narrow-band noise appears, and thus our new estimate is slightly different than reported earlier.[7]

We have observed narrow-band-noise spectra both at 110 and 77 K in the current-flow NMR sample. At 110 K the spectra consist of several closely spaced peaks, and their harmonics. The observation of several peaks is consistent with a variation among individual crystals in the sample. At 77 K the noise peaks are more rounded, which masks the structure of the peaks. Figure 2 shows a noise spectrum obtained at 77 K. The lower trace is the spectrum with no sample voltage, and the upper trace is the spectrum with a sample bias of 711 mV/cm. The structure common to both traces is external noise. A prominent fundamental is observed, as is its harmonic, along with a broad, enhanced noise background. A small third harmonic can also be observed, but is not apparent in this figure.

III. THE NORMAL STATE

In studies of the NMR above 144 K, where no CDW is present, we have observed spectra characteristic of the three Nb sites, at fields in the range 25–84 kG. Figure 3 shows the full quadrupolar spectrum obtained at 175 K, at 52.479 kG, with the orientation $\mathbf{H}_0\|\mathbf{b}$. These spectra have the form of nine equally spaced lines per site, as expected for spin-$\frac{9}{2}$ ^{93}Nb, although some of the outlying transitions are out of the range of the figure (beyond the tuning range of the probe).

The central lines of the spectra (resulting from the $m=\frac{1}{2}$ to $-\frac{1}{2}$ transitions) are closely spaced and sharp, typically 5 kHz wide in the orientation $\mathbf{H}_0\|\mathbf{b}$, at fields

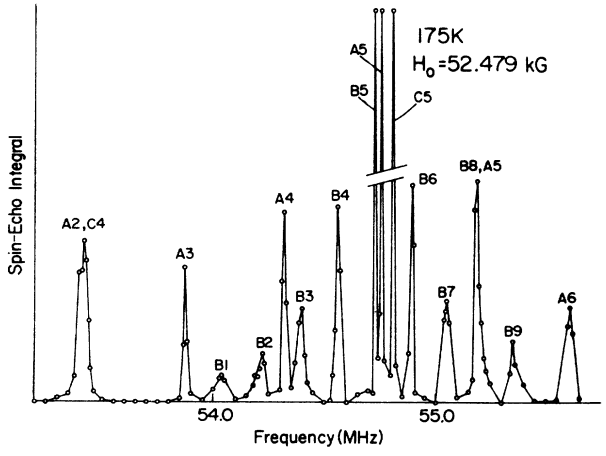

FIG. 3. Full quadrupolar ^{93}Nb spectrum of $NbSe_3$ in the normal state, in the orientation $\mathbf{H}_0\|\mathbf{b}$. The lines are labeled according to the sites *A*, *B*, and *C*; structural identifications are given in Table I. Some of the satellites are beyond the range of the spectrum. The central lines are the three tallest lines at the center.

used in our laboratory, and somewhat broader in other orientations due to the orientation distribution in the *a-c* plane. We have measured these central transitions extensively in field- and orientation-dependence studies. From the field dependences we separated the Knight shift and quadrupole shift at each site, and from the orientation dependences we determined the symmetry of these shifts.

The magnetic fields were measured using the ^{79}Br resonance (gyromagnetic ratio 1.0667 MHz/kG) in a KBr field marker. We used the value 1.0405 MHz/kG for the ^{93}Nb gyromagnetic ratio, taken from Carter *et al.*[12] This value differs somewhat from the Varian table value (1.0407 MHz/kG), which must be considered in comparing our Knight-shift values to, for instance, those of Devreux.[8]

The results of our measurements at 175 K are summarized in Table I. In the table the sites are identified as sites "*A*," "*B*," and "*C*," and also by the corresponding structural sites, according to our analysis described below. Electric field gradients (EFG's) are given in MHz (units of ν_Q); conversion to electromagnetic units requires multiplication by $2I(2I-1)h/3Q$, which is 4.31 (electrons Å^{-3})/MHz for Nb. V_{bb} and K_{bb} refer to the principal values of the EFG's and Knight shifts, respectively, along the *b* axis, which is a principal axis by symmetry. Note that this portion of our data corresponds to and agrees with the values of Table I in Ref. 8. The other two principal axes are described here as "α" and "β" for the EFG's, and "γ" and "δ" for the Knight shifts. (The axes α, β, γ, and δ differ from site to site.) The orientation of the principal axes in the *a-c* plane is specified by the angle between *c* and α, or γ. The sign of this angle is unknown since the aligned sample contains two sample orientations.

Our identification of the spectral sites is as follows: The EFG's result from the lattice charge, not only the electrons near the Fermi surface, so the EFG principal-axis symmetry should be indicative of the local structure. If one considers the nearest-neighbor selenium atoms at each Nb site (see Fig. 1), there is a pseudoreflection plane bisecting each triangular Se cage. For the red and orange sites, this plane cuts the *a-c* plane nearly perpendicular to *c*, while for the yellow site the angle is roughly 40°. We find that site *A* has a principal axis oriented ~43° from *c*, while the other two have axes more closely perpendicular to *c*. Thus, we associate site *A* with the yellow site. The other two sites cannot be distinguished on the basis of symmetry. Sites *A* and *B*, though, have nearly identical Knight shifts, which implies that they are almost equivalent electronically. Since it has been suggested[5,13] that the yellow and orange sites should have nearly equivalent conducting properties, whereas the red site is nearly insulating, we assign site *B* to the orange site and site *C* to the red site. These assignments are identical to those of Wada *et al.*,[9] based on changes in the relaxation times.

Comparison of the results reported here with the NQR study[10] shows that sites *A* and *C* correspond to the two sites observed in that study, whereas the orange site has EFG's too small to have been observed in the NQR study. Site *A*, which we identify as the yellow site, was

TABLE I. Measured ^{93}Nb electric field gradient (EFG) and Knight-shift tensor elements of $NbSe_3$ in the normal state, at $T=175$ K.

	A =yellow	B =orange	C =red
	EFG		
V_{bb} (MHz)	0.435±0.002	0.165±0.002	1.40±0.01
V_{aa} (MHz)	0.517±0.025	0.500±0.025	−0.05±0.025
$V_{\beta\beta}$ (MHz)	−0.952±0.025	−0.665±0.025	−1.35±0.025
c-α angle (deg)	±(43±5)	±(80±5)	±(70±5)
η	0.086±0.030	0.50±0.06	0.93±0.03
ν_Q (MHz)	0.952±0.025	0.665±0.025	1.40±0.01
	Knight shift		
K_b (%)	0.234	0.200	0.34
K_γ (%)	−0.057	−0.034	0.14
K_δ (%)	0.080	0.065	0.14
c-γ angle (deg)	±20	0	
K_{iso} (%)	0.086	0.077	0.207
η_K	0.93	0.80	0.00

also identified as the yellow site in the NQR study, and is the site which exhibited large changes below 144 K in zero field. The site which we identify as red, though, had previously been tentatively identified as the orange.

Devreux[8] has noted that the large Knight shift observed for site C is consistent with a nearly insulating red site, since it may be due to an orbital shift. The smaller Knight shifts at the other two sites can be traced to an orbital shift plus a smaller, negative core-polarization term.

Further evidence that the red site is, indeed, insulating is obtained by comparing the observed EFG's to values calculated numerically. We have calculated the lattice contribution to the EFG's by assuming ion charges having values given by Wilson[5] collapsed into point charges at the ion positions. Ion-charge values assumed are $-2e$ for unpaired Se, $-1e$ each for paired Se, $+5e$ for the red Nb, and $+4.5e$ each for the yellow an orange Nb. Unit cells were included up to and including the fifth-neighbor cell along b, and the second-neighbor cell along a and c. The ion positions were taken from Hodeau *et al.*[14] We used $\gamma_\infty=-15$ for the Sternheimer shielding factor.[15] The calculation was performed with no screening, and also with a simple (isotropic) Thomas-Fermi electron screening.

The lattice EFG calculated for the red site, with no screening, has $\nu_Q=+1.3$ MHz and $\eta=0.85$, with the maximum gradient along b. This is very close to the observed EFG-tensor principal values and orientation for site C. The addition of screening changes the calculated result very little. On the other hand, the lattice EFG calculated for the yellow site is nearly axial, with its maximum gradient along b, and $\nu_Q=+1.7$ MHz. This disagrees with the observed EFG symmetry for site A (or for the other sites). The calculation for the orange site also fails to reproduce the observed EFG's.

This apparent discrepancy can be rectified by the addition of a conduction-electron field-gradient term to the lattice EFG terms of the orange and yellow sites. For a quarter-filled d_{z^2} orbital along the b axis, the EFG will be axial, with the maximum gradient long b. Using a conduction-electron shielding factor $R=0.1$,[15] we estimate a quarter-filled d_{z^2} orbital to give $\nu=-1.9$ MHz. This is nearly equal and opposite to the calculated lattice term for the yellow site. Thus the orange- and yellow-site EFG's presumably represent the difference between lattice and electron terms of comparable magnitude. The red chain, on the other hand, can be modeled as nearly insulating, with the lattice term alone giving a satisfactory account of the observed EFG's.

IV. CDW LINE-SHAPE BROADENING

Below 144 K, which is the larger of the two CDW transition temperatures, we observe broadening of the lines corresponding to the yellow site. For the quadrupolar satellite lines, the broadening is so large that they disappear a few degrees below the transition. The central transitions for the yellow site, though, exhibit a definite structure which we have been able to resolve and analyze.

Devreux[8] has also observed the disappearance of the quadrupolar structure for one of the sites below 144 K. In contrast to that work, though, we find no change in the EFG tensor for either of the other two sites in this temperature range, since the orange and red central lines are unchanged by the transition in all sample orientations.

Figure 4 shows the central transitions in the orientations $\mathbf{H}_0\|\mathbf{b}$, at 52.478 kG, as the temperature is lowered through the 144-K CDW transition. The change in the yellow-site line is readily apparent. In orientations other than $\mathbf{H}_0\|\mathbf{b}$, the CDW-induced structure of the yellow central line is less clear due to the extra broadening caused by the small crystal-alignment distribution in the

a-c plane. Therefore, we have based our CDW-structure analysis largely upon the central lines observed in the orientation $\mathbf{H}_0\|\mathbf{b}$.

We have observed the field dependence of the CDW-broadened central lines at several temperatures in the range 65–135 K, for the orientation $\mathbf{H}_0\|\mathbf{b}$. The field variation allows separation of the Knight-shift contribution from the second-order quadrupole contribution to the line shape. At temperatures of 95 K and below, the width (in frequency) of the yellow line varies nearly as $1/H$, indicating that the broadening is predominantly quadrupolar.

In contrast to our observation of a quadrupole-broadened line for the yellow site, the NQR data[10] show a large change in field gradients for one site below the transitions, but with sharp lines. These results can be reconciled if the quadrupole broadening at the yellow site is due to a modulation in the orientations, but not the principal values of the field gradients, since the NQR spectra depend only on principal values.[16] We find that our line shapes, observed for the orientation $\mathbf{H}_0\|\mathbf{b}$, are consistent with such an orientation modulation in the field gradients. This model of the broadening mechanism will be referred to here as the "rotated-field-gradient" model.

In our rotated-field-gradient model the CDW broadening is given by a purely orientational modulation of the EFG's at the yellow site. The b crystal axis lies in the x-z plane of the EFG principal axes, and the principal axes are modulated so that x oscillates about b. [These principal axes are defined in the usual sense, so that $|V_{zz}|$ is the largest field gradient, and $(V_{xx}-V_{yy})/V_{zz}>0$.] Thus, for our studies with $\mathbf{H}_0\|\mathbf{b}$, the polar angles of H_0 with respect to the EFG principal axes are $\phi=0°$ and $\theta=90°+\Delta\theta(r)$, where $\Delta\theta(r)$ provides the inhomogeneous orientation distribution. While good agreement was obtained in this model with ϕ fixed at zero, an additional ϕ modulation might also yield reasonable agreement, with the limitation that x must rotation through b (where $\phi=0°$ and $\theta=90°$). Sample calculations showed that the ϕ modulation cannot be larger than 45° and the θ modulation must be at least 20° (for the 77-K line).

Good fits to the 77- and 95-K data were found using

$$\Delta\theta=\alpha\cos(\varphi_{\mathrm{CDW}}) , \tag{1}$$

along with EFG principal values consistent with the NQR results. Here, φ_{CDW} is the CDW phase, which advances linearly, and α is the amplitude of the orientation modulation. The principal values and axis orientations were combined with the usual formulas for the second-order quadrupole shift,[16] and the resultant inhomogeneous broadening was plotted numerically. A small Knight-shift modulation was also added to account for the small observed Knight-shift variation across the yellow line indicated by the field-dependence studies. This term has the form

$$K=K_0\cos^2(\varphi_{\mathrm{CDW}})+K_1\sin^2(\varphi_{\mathrm{CDW}}) . \tag{2}$$

This term has little effect on the line shape, giving only a small scaling of the width.

Line shapes given by this model are plotted in Fig. 5, along with data from 77 and 95 K. Parameters used for 77 K are $\nu_Q=1.18$ MHz, $\eta=0.60$, $\alpha=30.0°$, $K_0=0.258\%$, and $K_1=0.266\%$; for 95 K, $\nu_Q=1.176$ MHz, $\eta=0.60$, $\alpha=27.8°$, $K_0=0.253\%$, and $K_1=0.265\%$.

An even better fit than outlined above was obtained by replacing the simple sinusoidal EFG orientation modulation with a term containing a small amount of second harmonic. The form of the orientation distribution is then

$$\Delta\theta=\alpha[A_1\cos(\varphi_{\mathrm{CDW}})+A_2\cos(2\varphi_{\mathrm{CDW}})] . \tag{1'}$$

A good fit in this approximation was obtained with $A_1=0.96$ and $A_2=0.04$, for both temperatures, with all other parameters remaining the same. This is plotted in Fig. 5 with the dashed curves. The inclusion of the second harmonic is consistent with the observation[3] of a small second harmonic of the superlattice peak in x-ray-scattering studies.

The field-gradient rotations proposed certainly cannot correspond to physical twisting of the chains at large angles. On the other hand, we found that the yellow EFG's in the normal state result from a near-cancellation of two terms of comparable magnitude (see Sec. III), and thus large changes in the observed EFG's could result from

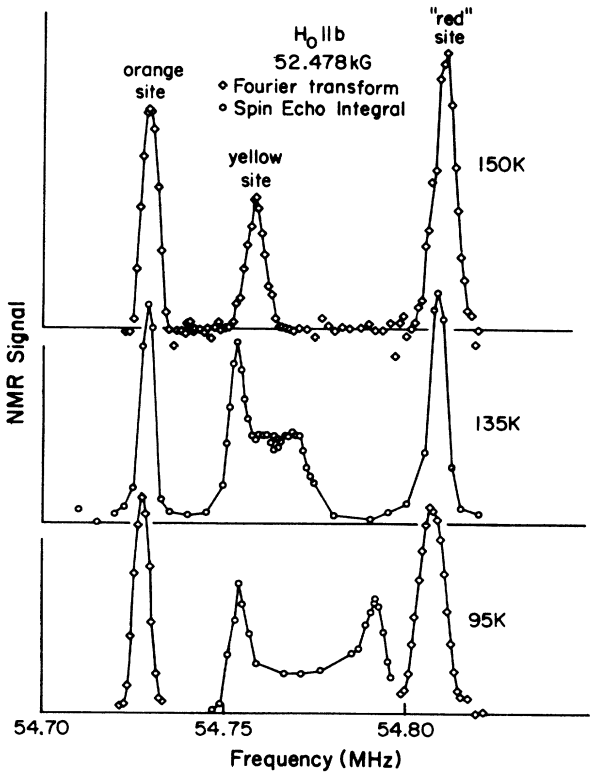

FIG. 4. Central lines at temperatures above and below the 144-K CDW transition, demonstrating the CDW-induced broadening of the yellow line.

smaller changes in either term. Indeed, we calculate that reasonable choices for modulated electron counts and ion displacements can give EFG's like those we observe, using the approximate numerical methods described in Sec. III.

The phasing of the EFG orientation modulation relative to the CDW in Eq. (1) is chosen such that the EFG modulation is linear in the CDW modulation. It is possible, though, that the EFG phasing varies as the square of the CDW modulation, since the second-order quadrupolar shift is proportional to ν_Q^2, containing terms both linear and bilinear in the charge deviation. The term $\varphi_{\rm CDW}$ in Eq. (1) would then be replaced by $2\varphi_{\rm CDW}$. Blinc[17] has successfully used a linear-expansion approach for incommensurate NMR line shapes, in which only the first- or second-order term of the quadrupole shift is kept; when only one term is important, the phasing can be deduced from the temperature dependence. This method is equivalent to our rotated-field-gradient analysis, but many terms would apparently be required here to achieve a good fit. The absolute phasing is therefore uncertain, and cannot be obtained from the incommensurate spectrum.

In addition to the phasing, we have assumed above a rigid incommensurate CDW phase profile. It is believed, though, that CDW phase distortions are central to the pinning of incommensurate CDW's. Such distortions can be due to the periodic lattice,[18] or to random impurities.[19] NMR is quite sensitive to lattice pinning and the appearance of discommensurations, as demonstrated by Suits *et al.*[20] A CDW characterized by very sharp discommensurations gives a splitting into discrete NMR lines, as opposed to the characteristic broadening of incommensurate CDW's.[20,17] For the intermediate case one expects a superposition of lines of the two types. Our line shapes show little or no evidence of discommensurations, as shown in the following analysis, and this indicates that the pinning mechanism of importance in $NbSe_3$ must be due to impurities.

To extend the line-shape analysis to include discommensurations, we have required the CDW phase, formerly uniform ($\varphi_{\rm CDW}=Qx$), to satisfy a sine-Gordon equation,

$$\frac{d^2\varphi(x)}{dx^2}=\alpha^2\sin\{4[\varphi(x)-\varphi_c(x)]\}\ , \tag{3}$$

after McMillan's[18] original proposal. Here, 4 is the nearest order of commensurability, $\varphi_c(x)$ is the rigid commensurate phase, and α is a parameter which, together with $\bar{\psi}_x=2k_F$, the average wave vector, determines the relative sizes of the commensurate and phase-slip regions. The limit $\alpha=0$ has no commensurate regions, whereas the limit $\alpha=\infty$ has infinitely sharp discommensurations.

Line-shape fits using this formula are plotted in Fig. 6, for three values of α. The inset in this figure shows the CDW phase minus the commensurate phase, corresponding to these values of α. Horizontal regions in the inset curves correspond to commensurate regions. As can be seen, the best agreement is found for the nondiscommensurate case ($\alpha\approx 0$). From these results, we place an upper limit of $\alpha=1.5$, which represents the middle curve in Fig. 6, with only very little phase distortion. The units of α are defined such that the distance between discommensurations is 2π. These results demonstrate that discommensurations are unimportant in $NbSe_3$, above 77 K.

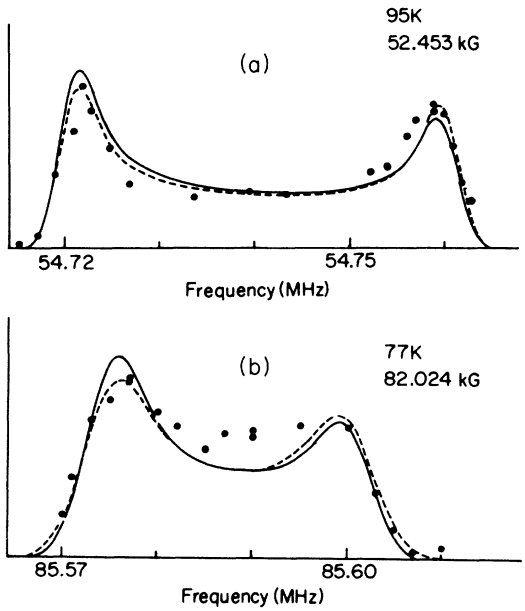

FIG. 5. The CDW-broadened yellow line, with theoretical curves obtained using rotated-field gradients, as described in the text. The dashed curves include a small second harmonic [Eq. (1')]. These fits contain no discommensurations.

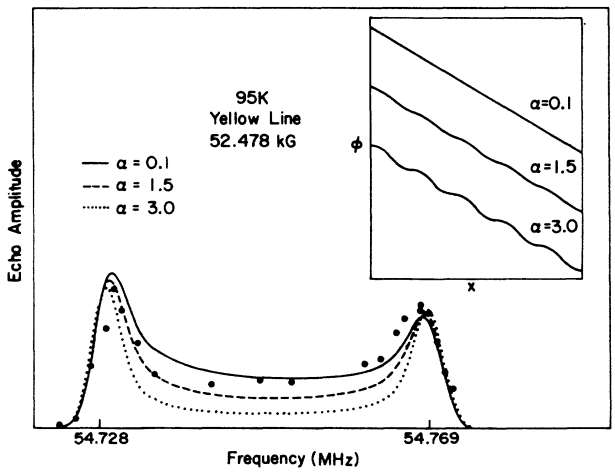

FIG. 6. Line-shape fit incorporating discommensurations. The inset shows phase profiles with different amounts of commensurability pinning. Calculated curves in the main graph are compared to data for 95 K and 52.478 kG.

Our estimates of the discommensurability rely on the local nature of the NMR shifts. There are, however, important nonlocal contributions to the EFG's due to the lattice charges. Numerical estimates of these contributions (similar to the numerical estimates reported in Sec. III) indicate that a very sharp discommensuration will have its width apparently stretched by, at most, three lattice constants on each site. For a wider discommensuration (as observed here), the effect will be less prominent. Since the discommensuration spacing for $NbSe_3$ will be at least 28 lattice constants, these considerations should not affect our conclusions.

The above discussion has involved commensurability pinning to the nearest commensurate phase, with a CDW wavelength of four lattice constants. It is also possible that the CDW may be commensurate to higher orders, even though the lock-in energy should decrease exponentially with the order of commensurability.[21] In this case, the broadened yellow line will be a superposition of a large number of discrete lines. These discrete lines should have the same intrinsic width as is observed on the orange and red lines, or, alternatively, that which can be estimated from the width of the sharp edges of the yellow line shape. In order to approximate the observed line shape, we numerically superimposed a set of such lines with a cosine distribution, $\nu(n)=\nu_0+\nu_1\cos(2\pi n/N)$, where n goes from one to N, and N is the order of commensurability. Plotting these curves, we discover that the line shape becomes smooth (and thus could approximate the observed data) for $N \geq 22$. This gives an estimate of the lowest order for which commensurability may exist in $NbSe_3$ above 77 K.

V. NMR WITH CDW MOTION

By studying the NMR spectra with simultaneous current flow, we have probed the local motion of the CDW. These studies were performed with a sample which has 30 crystals connected in parallel between common electrical leads. More information about this sample is given in Sec. II. The sample orientation is $\mathbf{H}_0 \| \mathbf{b}$ only; this is the orientation for which we obtained well-resolved CDW line shapes, as shown in Figs. 4–6. The measurements were performed at 77 K, with the probe immersed in liquid nitrogen. This offers temperature stability,and heat sinking for any Ohmic heating in the sample.

The magnetic field for the experimental runs was fixed at 84.533 kG. The yellow central line shape at this field and 77 K is essentially the same as shown in Fig. 5(b). The linewidth is 30 kHz, and the intrinsic (non-CDW) linewidth is 8 kHz. The intrinsic linewidth is found by measuring the linewidth of the red and orange lines in the same field, and this width produced a good fit to the yellow line shape when convoluted with the theoretical CDW broadening of Sec. IV.

A. Motional narrowing

Motional narrowing[22] refers to the collapse of NMR spectra into narrow lines because of time averaging during local motion. The observation of motional narrowing gives an unambiguous demonstration that the CDW is in bulk translational motion at large applied voltages. The effect is demonstrated in Fig. 7(a), showing spin echoes due to the yellow central line obtained with and without voltage applied to the sample. (The high-frequency oscillations in these echoes are due to the neighboring red and orange lines.) With no applied voltage (lower curve), the echo is narrower, corresponding to a broader line shape,[22] and it has oscillations due to the edge peaks in the line. With 100 μA flowing through the sample (which corresponds to 1.4 V/cm), though, the echo becomes broad, and the structure changes. Thus is demonstrated the line-shape change characteristic of motional narrowing. Motional narrowing has also been observed in NMR studies of the CDW conductor $Rb_{0.3}MnO_3$,[23] indicating that it also exhibits bulk CDW motion.

The echoes of Fig. 7, as well as subsequent data, represent echoes recorded in repetition and signal-averaged. The time between echoes was 30 ms. The spin-echo sequence typically lasts 200 μs; for Fig. 7, the pulse separation was 150 μs. The sample voltage was applied only for the duration of the echo sequence; it was turned on 10 μs prior to the 90° pulse, and turned off after observing the echo. In this manner, saturation effects (described below) are avoided. The sample current was measured by observing the voltage across a series resistor external to the NMR probe. This external resistor was larger than the sample resistance, making the supply effectively a constant-current source. The sample voltage is extracted from the measured current using the separately measured I-V curve.

We have followed the line narrowing versus sample voltage by measuring the echo shape. The results are plotted in Fig. 7(b). Here the spin-echo delay time (time between 90° and 180° pulses) was 150 μs. The linewidth is defined as $(2\ln 2)/(\pi t_{1/2})$, where $t_{1/2}$ is the half-width at half maximum (HWHM) of the echo. This gives the full width at half maximum (FWHM) of a Gaussian line shape, and serves as a relative measure of the line narrowing for our more complicated line shape.

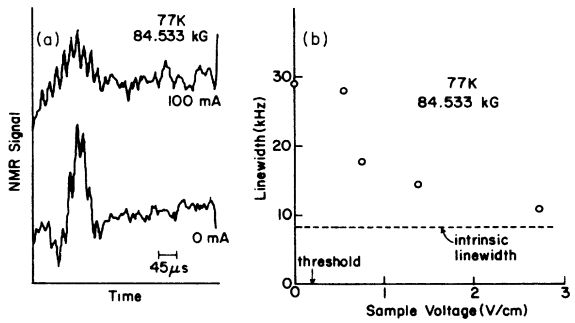

FIG. 7. Motional-narrowing results. (a) Spin echoes obtained with and without sample voltage applied. The broader echo indicates a motionally narrowed line. (b) The linewidth vs sample voltage.

The intrinsic linewidth, indicated in the figure, represents the width of the red and orange central lines at the same field, measured in the same way. This intrinsic width is predominantly due to dipolar interactions. We find that the yellow linewidth approaches this intrinsic linewidth at large sample bias. Thus, to within our detection limit defined by the dipolar coupling, the CDW contribution to the linewidth is removed by the applied sample bias. Since the NMR signal is a superposition of signals from the entire sample, this result implies that the applied current affects essentially all parts of the sample.

Motional narrowing is most familiar in liquids,[22] in which rapid bodily motion of molecules modulates the dipolar and other couplings, causing a narrowing of the rigid-lattice linewidth. In our case, only the CDW distortion moves, causing a modulation of the associated field gradients (EFG's), but not the dipolar couplings. Therefore, the reduction of the yellow linewidth to the intrinsic (dipolar) width is consistent with CDW motion.

There is a small enhancement of the measured linewidth in Fig. 7(b) as compared to the intrinsic value, even at the largest applied sample voltage. This can be attributed to some portions of the sample remaining stationary. Comparing the relative amount of linewidth reduction, these portions amount to on the order of 10% of the sample. This may well result from a few crystals having poor contacts. (The crystals are more or less uniform in current density, as evidenced by our observations of narrow-band-noise peaks, with three harmonics, and a well-defined distribution of non-Ohmic conduction thresholds, distributed between 100 and 200 mV/cm at 77 K, in the actual NMR sample.) On the other hand, this could indicate motion variations within the crystals; we cannot distinguish these possibilities at present. Clearly, though, the CDW motion encompasses the major portion of the sample.

Since the CDW is a periodic distortion, CDW motion will produce periodic changes in the NMR frequencies, not random changes, as in the liquid case. Strict periodic motion will transform the NMR line into a fundamental with associated sidebands. The fundamental will be observed at the time-averaged NMR precession frequency, and the sidebands will be spaced by the CDW motion frequency. This is the same phenomenon observed in FM modulation in radio. Kogoj *et al.*[24] have numerically examined such spectra in the perfect uniform CDW motion limit, and also in the limit of strong discommensuration motion. In the latter case, the spectra become rich in structure, with many juxtaposed narrow lines. This structure, though, could easily be obscured by a small amount of broadening from other sources. In addition, macroscopic variations in CDW velocity will broaden the sideband structures, and may also thus obscure the lineshape structure.

We see no evidence for sideband structure in our sample. We note, though, that the dipolar broadening represents a sizable fraction (about $\frac{1}{4}$) of the total (static) linewidth. Thus any complicated intermediate line shape caused by the CDW modulation will simply be washed out. Also, we mention the recent observations of lineshape structure in studies of the blue bronze,[23] indicating possibly more uniform motion in that material at low temperatures.

For simple models of CDW motion, one expects that the NMR line will narrow when the CDW-motion frequency equals approximately the static linewidth, which, in our case, is 30 kHz. This is the case for random motions in liquids,[22] and also for uniform periodic motion,[24] in which the sidebands discussed above become small once they exceed the boundaries of the static line shape. (There is, as mentioned in Sec. IV, some uncertainty as to whether the NMR broadening is proportional to the CDW order parameter or its square, and, if the latter is the case, narrowing should occur when the CDW-motion frequency exceeds half the static linewidth, or 15 kHz.)

In contrast to these expectations, narrowing is not observed here until the apparent CDW-motion frequency far exceeds the static linewidth. The narrowing commences at about 0.55 V/cm [the inflection point in Fig. 7 (b)], but at this field the narrow-band-noise peaks are observed in our sample well into the MHz region. At 0.25 V/cm, a broad noise peak is observed centered at 3 MHz, and at 0.41 V/cm the peak has moved to 10 MHz. An estimate based on the measured excess CDW current (using a charge density of two electrons per chain per CDW wavelength, and our estimate of the sample cross section) yields a 1.5-MHz CDW frequency at 0.55 V/cm. Thus we have reasonably consistent estimates of the CDW motion frequency, and this estimated frequency is much larger than the NMR linewidth.

We have observed some dependence of the motional-narrowing curves on the delay time (the time between spin-echo excitation pulses). This effect is due to the much shorter T_2 (spin-echo decay time) for the motionally narrowed line than for the static line. As the delay time is increased, the amplitude of the narrowed line decreases, giving more weight to the un-narrowed portion. A sample inhomogeneity consistent with the width of the noise peaks in our sample is sufficient to explain the observed effect. At the delay time used for Fig. 7, the narrowed signal is reduced in amplitude by approximately $\frac{1}{2}$, which will give only a small change in the data compared to what would be expected if there were no motion dependence to the T_2.

One can argue that the observed noise peaks in our sample result from a small fraction of the sample with a fast-moving CDW, while most of the sample has a much more slowly moving CDW. This would explain the discrepancy in the expected versus observed sample current required to narrow the line shape. Such an effect, though, should be apparent in our measurements of the excess CDW current as a large discrepancy between the CDW frequency measured this way and the noise-peak frequency. Moreover, our saturation results (see below) indicate that the CDW response in our sample is quite uniform. Rather, our data support CDW motion that is nonuniform in time, but approximately the same throughout the sample. In our interpretation, at low velocity, the CDW moves in quick jumps, separated by times when the CDW is nearly stationary. The jumps likely occur at different times in different domains. This

picture, then, is not unlike the numerical simulations of Littlewood,[25] and also the theory of Tucker *et al.*,[26] both based on strong impurities. When motion frequencies are small compared to ω_L, the NMR signal can be described as an integral,

$$S(t)=S_0 \exp[i(\omega_L-\omega_{\rm rf})t]\left\langle \exp\left[i\int \Delta\omega(x,\tau)d\tau\right]\right\rangle , \quad (4)$$

where the angular brackets represent an average over x, and $\Delta\omega$ represents the local instantaneous NMR precession frequency (referenced to the Larmor frequency ω_L). Thus if the CDW exhibits a "jerky" motion as described above, it will spend much of its time at a given local phase, mod 2π, fixed by the local pinning centers. In this case, the integral in (4) will be heavily weighted by the stationary time periods, and the signal will differ very little from the static signal, even though the average CDW-motion frequency may exceed the classical narrowing criterion. This result relies on the fact that the NMR frequency is periodic in the CDW phase. On the other hand, if the CDW motion goes over to a smooth phase advance, narrowing will be seen in the usual sense.

In our model, then, the CDW motional narrowing occurs when the CDW motion goes over from a jerky type of motion to a smooth motion at voltages far exceeding the conduction threshold. This interpretation agrees with both the motional-narrowing results and the saturation results, described below. We assume that the phase advance at low motion speeds requires a time $T_{\rm ph}$, perhaps limited by dissipation in the normal electrons, but at high motion speed the phase cannot adjust, and advances smoothly. The crossover will be at an average CDW-motion frequency of $1/T_{\rm ph}$. We observe narrowing at an approximate motion frequency of 10 MHz, which implies that $T_{\rm ph}=0.1\ \mu$s.

B. T_2 measurements

Due to signal-to-noise limitations, spin-echo T_2 measurements were limited to a few points, but clearly indicate that the T_2 is much reduced with large current flows.

The T_2 is measured by observing the decay of the spin-echo amplitude versus the delay between pulses. The echo refocuses static field inhomogeneities, but decay can be due to (i) mutual spin flips caused by the dipolar or pseudodipolar interactions, (ii) T_1-type spin-flip processes, or (iii) motions which change the spin evolution.

The static spin-echo decay of the yellow central line was measured at 77 K with the large aligned sample. The decay is neither Gaussian nor exponential, but is well fitted by a sum of functions which is 70% Gaussian and 30% exponential, with a signal reduction of 50% at $2\tau_D=2.1$ ms. T_1 has a time constant of 20 ms at 77 K, so lifetime broadening is unimportant to the observed T_2.

By using a Ruderman-Kittel[27] Hamiltonian and the value[28] $\nu_{\rm HFS}=7050$ MHz, we estimate the nearest-neighbor J coupling for the yellow site to be 6 kHz. Neighbors not in appropriate m states, though, will be energetically denied mutual spin flips because of the large static quadrupole field. Thus the decay will be reduced from the above value. The exact calculation has not been performed for the $NbSe_3$ lattice, but it seems that mutual spin flips due to the static J coupling give a reasonable accounting for the observed decay function.

In measurements taken with the moving CDW, T_2 is consistently shorter than in the static case. This persists to the highest voltage applied, 2.0 V/cm, at which the narrow-band-noise fundamental peak is observed at 80 MHz. Figure 8 shows the data. These data were measured using the same technique as above; the rf-pulse separation was varied, and the echo amplitude recorded. The sample current was switched on 100 μs prior to the first pulse, and kept on until after the echo was recorded. The sequence was repeated at 30-ms intervals and signal-averaged.

All the data of Fig. 8 were obtained using the same sample. The static decay function (dashed curve) is shown fitted to the data obtained with no current. With applied voltages of 0.55, 0.72, and 2.00 V/cm, at which significant line narrowing was observed, the decay is much faster. Also apparent is that the applied-current data represent a signal equal or nearly equal in amplitude to the static signal, when corrected for the relaxation. The solid curve, which represents an exponential decay with $T_2=250\ \mu$s, is included to indicate the approximate time scale for the motion-induced relaxation.

Since the amplitude of the echo, extrapolated to zero delay between pulses, is proportional to the number of resonant spins observed, it is apparent that the motionally narrowed signal represents all or most of the spins observed with no applied current. We can say that at least half of the sample is observed in the motionally narrowed signal. This rules out any model in which only small sections of the CDW are actually in motion, showing instead that the CDW motion involves the entire crystal.

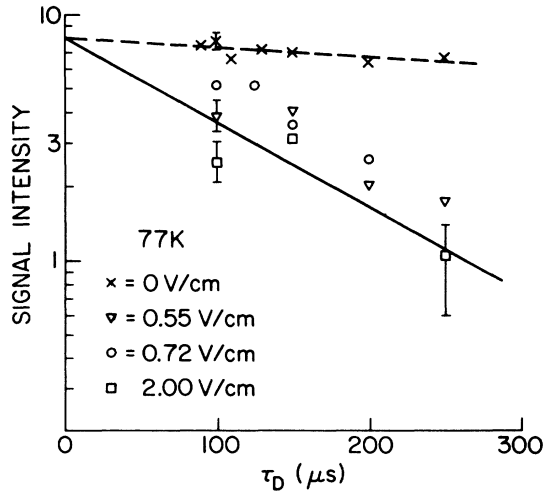

FIG. 8. T_2 measurements for various applied voltages. The dashed curve is the zero-voltage T_2 decay. The solid curve, an exponential decay with $T_2=250\ \mu$s, is the approximate decay for the moving CDW, described in the text.

In the classical theory of motional narrowing,[29] the linewidth $(1/T_2)$ is constant until the motions become fast enough to commence motional narrowing, at which point T_2 becomes larger. For spin echoes, a *reduction* in T_2 can be caused by diffusion of molecules in a field gradient,[30] as the NMR frequencies for a diffusing molecule are slowly changed. The T_2 will again grow longer once the diffusion time becomes shorter than the natural decay time, giving motional narrowing. In the present case, NMR frequencies are changed by the motion of the CDW, and the reduced T_2 implies that the motion contains quasistatic components, homogeneously throughout the sample. This leads to a surprising result, namely that even at the largest voltages applied to the sample, when the average CDW motion frequency is 100 MHz, the motion contains intermittent slow motions which reduce the T_2. This also explains the limiting linewidth in measurements of the blue bronze.[23]

C. CDW-induced saturation

As another manifestation of the moving charge-density wave, we have observed a saturation of the NMR signal induced by the application of a steady current to the sample. Figure 9 demonstrates the effect. Plotted are the equilibrium NMR signal versus the sample bias, all measured at 77 K. Usually, a NMR sample will give an equilibrium signal determined only by the number of spins and the temperature (through the Boltzmann population function). The change in equilibrium signal observed here indicates that the CDW current can drive the spin populations out of equilibrium by inducing spin flips.

These measurements were performed by signal-averaging repetitive spin echoes, as before, but this time a steady current was turned on only during the waiting time between echoes. The current was turned off during the time required to measure the echo; this simplifies the analysis by avoiding current-induced line shape and T_2 changes. Each echo experiment destroys the magnetization, so by observing the signals for different waiting times, the saturation-recovery properties can be measured.

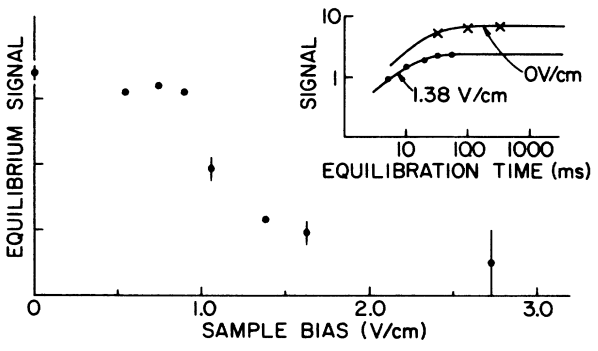

FIG. 9. Current-induced saturation of the magnetization. The inset shows the recovery curves measured with no applied voltage and with 1.38 V/cm. The shape of the zero-voltage recovery is taken from measurements using the large sample. The main graph shows the equilibrium magnetization vs sample voltage and illustrates a saturation threshold near 1.0 V/cm.

The inset to Fig. 9 shows the recovery curves with no applied sample bias, and with 1.38 V/cm applied. With no applied bias, the T_1 recovery time at 77 K is 20 ms; the data shown were measured using the current-flow sample, and the fit is the recovery curve measured with the larger sample. With 1.38 V/cm sample bias, the recovery is quite different. At long times, the equilibrium signal is reduced from the no-current value. In addition, the recovery is faster. The lower curve is an exponential with a T_1 of 11 ms.

With a random-spin-flip process, such as would obtain for rf irradiation, a spin system can be described by the rate equation[22]

$$\frac{dn}{dt} = -(1/T_1)(n-n_0) - 2Wn \ , \tag{5}$$

where n represents the magnetization density, with n_0 its equilibrium value in the absence of irradiation. The first term on the right represents a thermal (single-exponential) T_1 process, and W is the spin-flip probability for the external irradiation. The solution appropriate to the saturation-recovery experiment is

$$n(t) = n_{\text{eff}}[1 - \exp(-t/T_{\text{eff}})] \ , \tag{6}$$

where $n_{\text{eff}} = n_0/(1+2T_1W)$, and $T_{\text{eff}} = T_1/(1+2T_1W)$. The apparent T_1, and the equilibrium magnetization n_0, are reduced by the same factor. This is borne out in the results shown in the inset of Fig. 9, for an applied bias of 1.38 V/cm, where the equilibrium magnetization is reduced by a factor 0.36 ± 0.05, and the apparent T_1 is reduced by a factor of approximately 0.55. Thus the observed signal reduction can be explained as saturation due to internal rf fields associated with the moving CDW. The signal reduction cannot be due to sample heating since the $NbSe_3$ crystals, a few micrometers thick and still metallic below the CDW transitions, are well heat-sinked by immersion in liquid nitrogen. Moreover, the T_1 is strongly influenced by phonons and decreases with temperature too rapidly to explain our observations; for instance, at 110 K the T_1 becomes 3 ms, but the signal strength would be reduced only to 70% of its 77-K value.

The main graph in Fig. 9 shows the equilibrium magnetization measured as a function of the sample bias applied during the waiting time. Clearly, there is a threshold near 1.0 V/cm above which the line begins to saturate. Above this value, the signal exhibits a reduction in signal with increasing bias until, at 2.7 V/cm, no signal was observed in 2 d of signal averaging. (During this average the collection was paused to verify the full signal strength at no sample bias.) No data were collected above 2.7 V/cm for fear of damage to the sample.

Comparison with measured narrow-band noise in our sample shows that the saturation threshold occurs when, at 77 K, the second harmonic reaches the NMR frequency, 88 MHz. A representative narrow-band-noise curve is shown in Fig. 2; we observe a broad fundamental and two harmonics at 77 K. At 1.0 V/cm the fundamental is

observed at 45 MHz, with a width (FWHM) of 8 MHz. The second harmonic, at 90 MHz, has a width of 16 MHz.

The matrix elements for spin-flip transitions can be calculated using our fit to the field gradients induced by the CDW, and we will demonstrate that these matrix elements are of an appropriate magnitude. The quadrupole Hamiltonian has both $\Delta m=1$ and 2 matrix elements. Because of the rotated EFG principal axes induced by the CDW, the matrix elements include many harmonics of the fundamental phonon frequency, in an expansion that is straightforward but omitted here. The lowest-order terms are proportional to

$$V_{\pm 1}=-h\nu_Q[(3-\eta)/4]\alpha\sin(\omega t)$$

and (7)

$$V_{\pm 2}=h\nu_Q[(3-\eta)/4]\alpha^2\sin^2(\omega t)\ ,$$

where α is the tipping angle in our rotated-field-gradient model, and $V_{\pm 1}$ and $V_{\pm 2}$ are proportional to the $\Delta m=1$ and 2 matrix elements, respectively, by factors of order unity. Both terms, then, will induce transitions when the phonon frequency equals the Larmor frequency.

Inserting parameters taken from the line-shape analysis of Sec. IV yields matrix elements of 0.6 and 0.8 MHz for the $\Delta m=1$ and 2 transitions, respectively, for uniform CDW translation. Assuming that this perturbation is not applied steadily, but fluctuates within the observed noise-peak width, the transition rate will be given by

$$W_{mn}=|\langle m|H|n\rangle/h|^2/W_{1/2}\ , \tag{8}$$

which follows from Fermi's "golden rule," given $W_{1/2}$, the width of the noise peak. For the fundamental noise peak, with a width of 8 MHz, this implies a transition rate of $W_{mn}\approx 100$ kHz. This is more than enough to overcome the thermal relaxation rate, $1/T_1=50$ Hz. Furthermore, if the observed second-harmonic noise-peak height (5% of the fundamental) reflects the amplitude of the $4k_F$ phonon, the second harmonic will have a matrix element, for the $\Delta m=1$ term, of 0.6 MHz$\times 5\%=30$ kHz. Then, taking the 16-MHz observed second-harmonic width, one obtains a transition rate of 60 Hz. The latter value is very close to the thermal-relaxation rate. The third harmonic would give a rate considerably smaller than the thermal-relaxation rate, thus insufficient to cause saturation of the NMR line.

We have, then, a satisfactory explanation for the observations. Near 1.0 V/cm, the $4k_F$ phonon frequency crosses the 88-MHz NMR frequency, inducing saturation of the signal. Were the CDW velocity narrowly defined rather than distributed over a broad range, the signal would be reduced only for a narrow range of current, in which the CDW-motion frequency precisely matched the NMR frequency. Instead, the signal is reduced for a broad range of currents. As the fundamental moves past 90 MHz, the saturation might be reduced at sufficiently large currents; this was not observed at the largest currents used here, and since there is noise signal observed continuously down to dc, it may be that there is sufficient spectral density that the saturation would continue at all larger currents.

We must make a distinction between fluctuations in the CDW motion frequency, and a fixed distribution of frequencies. The width of the noise peaks might be explained by either model, but our results are consistent with only the former, in which at each point in the crystal the CDW-motion speed changes with time, sampling the entire range of motion frequencies. In other words, the velocity broadening is homogeneous in our samples. This follows since the large observed reduction in signal (at least 80%) implies that a large fraction of the spins "see" fluctuations at the NMR frequency, which is inconsistent with a fixed spatial distribution of CDW velocities. A fluctuating CDW-motion velocity was also indicated by our T_2 results, described above, which indicated a highly nonuniform motion of the CDW. This may be associated with the thermal broadening of the noise peaks, which is observed at 77 K.

Although spin diffusion from the bulk of the crystals to a few domains with the proper motion frequency might also give this type of saturation, this mechanism is short-circuited by the thermal T_1 in $NbSe_3$. It can be shown that the range of magnetization reduction around a saturation center is approximately $(JT_1)^{1/2}$ sites, where J is the spin-spin coupling, essentially $1/T_2$. In our case we have $T_1=20$ ms, and $T_2=1$ ms, giving a range of approximately five sites, not enough to be significant. Therefore, we must have similar motion in all the domains in the sample, as implied above.

VI. CDW DISPLACEMENTS AT LOW SAMPLE VOLTAGES

In addition to investigating CDW motions above the conduction threshold, we have used a set of pulse measurements to study the displacements of the CDW within its confining potential at low sample voltages.

The rf-pulse sequence for these experiments consists of the Carr-Purcell-Meiboom-Gill sequence,[31] which consists of one 90° pulse followed by a series of 180° pulses. A spin echo is produced between each of the 180° pulses. We used an eight-echo sequence, separately digitizing and averaging each echo, then adding them. A weighting function equal to the T_2 decay function was used for the echo sum, to optimize the signal-to-noise ratio. The sequence was repeated at 30-ms intervals, as before, for signal averaging. To the rf-pulse sequence was added a voltage pulse applied to the sample in the interval between the 90° and 180° pulses, and also in some cases in the interval between the first two 180° pulses, before the appearance of the echo. The NMR frequency shift induced by these pulses alters the refocusing effect of the spin echo, and it is in this way that the CDW displacement could be probed.

In order to understand the effect of CDW displacements on the spin echo, we examine the line shape at the yellow site (Fig. 4). The edge singularities result from the frequency extrema in the CDW, points separated by a half-wavelength of the CDW. The spins contributing to the center of the line shape are at intermediate CDW points, separated from the edge singularities by roughly

one-quarter wavelength. Thus for a 90° phase shift of the CDW, spins at the center of the line move to the two edge singularities, and spins at the edges move to the center. This gives a maximum frequency shift of half the linewidth, or 15 kHz at 77 K and 84.5 kG. Since the frequency shifts depend on the spin position in the CDW, CDW displacements will cause destructive phasing in coherently precessing spins. Echo destruction should occur on a time scale of roughly $1/(2\times 15$ kHz) for a 90° displacement for our case, or 30 μs.

Applying voltage pulses between the 90° and 180° pulses, we have measured the integrated area under the summed spin echoes versus the pulse length. The integral of the echo selects a narrow band of signal at the excitation frequency, rather than the entire line shape. In Fig. 10 are shown results for voltage pulses of 150 mV at the sample, which corresponds to roughly the center of the distribution of threshold fields for our sample. The NMR observation frequency was at the center of the broadened CDW line. The experiment was carried out for pulses of up to 500 μs, which was the (fixed) delay between 90° and 180° pulses.

The observed decay was fitted numerically by an echo-simulation routine, using a plane-wave CDW model and a simple line-shape fit with no higher harmonics, as described in Sec. IV. In this fit it was assumed that the phase difference between line-shape maxima was 180°. While our NMR measurements do not measure this phase difference directly, it seems highly unlikely that this value would be other than 180° or 90°, but there remains a factor of 2 uncertainty.

The curves in Fig. 10 are curves calculated using this assumption, with constant phase displacement during the voltage pulse, and immediate phase relaxation upon turning off the voltage. The dotted and dashed curves assume a uniform phase advancement of 5° and 2°, respectively. The 2° curve falls close to the data at short times, but fails to agree at longer times. Much better agreement is given by the solid curve, which includes an average displacement of 2°, but with a Gaussian inhomogeneous distribution, of half-width 2°.

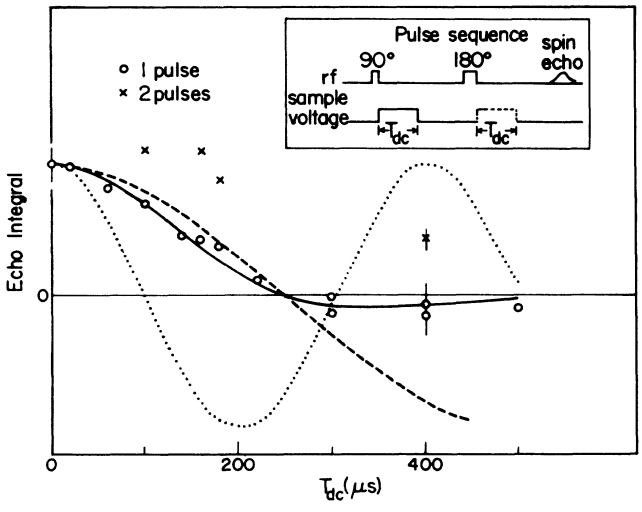

FIG. 10. Results from dielectric-displacement measurements. Data are integrals of Carr-Purcell echoes. The calculated curves, described in the text, include the following CDW displacements: uniform 5° displacement (dotted curve), uniform 2° displacement (dashed curve), and 2° average displacement with a Gaussian distribution (solid curve).

Our result, the 2° average displacement, depends on our choice of phasing, 180° between line-shape peaks. If the appropriate phasing were 90° between peaks, the result would be an average 1° displacement. Additional uncertainties would result from stray fields produced by the sample currents. Stray fields from the chokes on the current-supply lines will be approximately 0.1 G maximum, but the fields of the two chokes oppose to reduce the effect. A stray field of 0.1 G implies a frequency shift of 0.1 kHz during the pulse, or a defocusing time of 2 ms, much longer than that observed here.

In a classical single-particle model[32] the phase would respond by 90° at threshold, clearly much larger than our observations. In comparing other models, it is useful to compare the quantity ϵE_T, which is the total charge displacement at threshold, using the small-field dielectric response ϵ. For the classical single-particle model,[1] $\epsilon E_T = 2n_c e\lambda$, where n_c is the CDW charge density and λ is the CDW wavelength. Assuming $\lambda = 14$ Å and $n_c = 1.9\times 10^{21}$ cm^{-3} (using two electrons per chain per wavelength in $NbSe_3$) yields $\epsilon E_T = 7.7\times 10^7$ V/cm. The measured values of Grüner *et al.*[33] at 77 K yield $\epsilon E_T = 4.5\times 10^6$ V/cm, reduced from the rigid classical value by a factor 0.058. Our result implies a phase displacement reduced from the rigid classical value by a factor 0.02.

Assuming that the quantity ϵE_T is proportional to the phase displacement at threshold, the apparent discrepancy between our NMR result and the electrical measurements can be accounted for by a nonuniform phase response within the sample. Making the simplifying assumption that regions of the sample can be divided into those with a small dielectric response and those with a large dielectric response, the NMR response will show a fast decay followed by a slow decay. If the regions of fast decay were only a small fraction of the sample, they would contribute to the average dielectric response measured electrically, but the initial decay would be lost in the scatter of our data. For example, then, if the phase response were 90° at threshold in 4% of the sample and 2° in 96% of the sample, the average phase response would be 5.5°, agreeing with the apparent phase response measured electrically. Thus the small phase displacement that we measure can be explained in a simple model requiring inhomogeneous CDW displacement.

A number of more detailed theoretical studies yield results that support these experimental findings. Tucker *et al.*[26] have described a theory based on strong pinning which accounts for the magnitude of the phase displacement observed here. Dumas and Feinberg[34] propose a theory based on CDW dislocation which would also imply a strongly nonuniform phase response. In addition, in numerical simulations, both Littlewood[25] and Matsukawa and Takayama[35] have demonstrated nonuni-

form phase response in CDW motion that may be related to the motion described here.

VII. CONCLUSIONS

In this paper we have reported the results of a set of ^{93}Nb NMR experiments probing the electronic structure of $NbSe_3$ and the CDW motion. In the normal state, we have measured the full Knight shift and quadrupole tensors. The results give evidence for one essentially insulating site and two conducting sites. Below the transitions we have seen that the CDW's are localized on the yellow and orange sites. In NMR studies with simultaneous current flow we have observed the motional narrowing of the CDW line at the yellow site, and have seen current-induced saturation of the NMR, which provides a measurement of the motion frequencies. In addition, we have used pulsed NMR techniques to probe the dielectric response of the CDW.

ACKNOWLEDGMENTS

We acknowledge Bryan Suits for his work on the initial stages of this project, as well as for advice and discussions. We also acknowledge useful discussions with our colleagues George Mozurkewich, John Bardeen, J. R. Tucker, and R. E. Thorne. This research was supported by the U.S. Department of Energy, Division of Materials Research, under Contract No. DE-AC02-76ER01198.

---

*Present address: Department of Physics, Texas A&M University, College Station, TX 77843-4242.

†Present address: D501 Richards Building, University of Pennsylvania, Philadelphia, PA 19104.

‡Also at Department of Chemistry, University of Illinois at Urbana-Champaign, Urbana, IL 61801.

[1]G. Grüner and A. Zettl, Phys. Rep. **119**, 117 (1985).

[2]N. P. Ong and P. Monceau, Phys. Rev. B **16**, 3445 (1977).

[3]R. M. Fleming and C. C. Grimes, Phys. Rev. Lett. **42**, 1423 (1979).

[4]J. L. Hodeau *et al.*, J. Phys. C **11**, 4117 (1978).

[5]J. A. Wilson, Phys. Rev. B **19**, 6465 (1979).

[6]R. M. Fleming, D. E. Moncton, and D. B. McWhan, Phys. Rev. B **18**, 5560 (1978).

[7]Joseph H. Ross, Jr., Zhiyue Wang, and Charles P. Slichter, Phys. Rev. Lett. **56**, 663 (1986); Joseph H. Ross, Jr., Ph.D. thesis, University of Illinois at Urbana-Champaign, 1986 (unpublished).

[8]F. Devreux, J. Phys. (Paris) **43**, 1489 (1982).

[9]S. Wada, R. Aoki, and O. Fujita, J. Phys. F **14**, 1515 (1984).

[10]B. H. Suits and C. P. Slichter, Phys. Rev. B **29**, 41 (1984).

[11]A. Meerschaut and J. Rouxel, J. Less-Common Met. **39**, 197 (1975).

[12]*Metallic Shifts in NMR*, edited by G. C. Carter, L. H. Bennett, and D. J. Kahan (Pergamon, Oxford, 1977), Pt. I.

[13]Roald Hoffman *et al.*, J. Solid State Chem. **34**, 263 (1980).

[14]J. L. Hodeau *et al.*, J. Phys. C **11**, 4117 (1978).

[15]E. Ehrenfreund, A. C. Gossard, and F. R. Gamble, Phys. Rev. B **5**, 1708 (1972).

[16]M. H. Cohen and F. Reif, in *Solid State Physics*, edited by H. Ehrenreich, F. Seitz, and D. Turnbull (Academic, New York, 1957), Vol. 5, p. 322.

[17]R. Blinc, Phys. Rep. **79**, 5 (1981).

[18]W. McMillan, Phys. Rev. B **14**, 1496 (1976).

[19]H. Fukuyama and P. A. Lee, Phys. Rev. B **17**, 535 (1978); P. A. Lee and T. M. Rice, *ibid.* **19**, 3970 (1979).

[20]B. H. Suits, S. Couturie, and C. P. Slichter, Phys. Rev. Lett. **45**, 194 (1980).

[21]P. A. Lee, T. M. Rice, and P. W. Anderson, Solid State Commun. **14**, 703 (1974).

[22]Charles P. Slichter, *Principles of Magnetic Resonance* (Springer-Verlag, Berlin, 1980).

[23]P. Ségransan *et al.*, Phys. Rev. Lett. **56**, 1854 (1986): A. Jánossy *et al.*, *ibid.* **59**, 2348 (1987).

[24]M. Kogoj, S. Zumer, and R. Blinc, J. Phys. C **17**, 2415 (1984).

[25]P. B. Littlewood, Phys. Rev. B **33**, 6694 (1986).

[26]J. R. Tucker, W. G. Lyons, and G. Gammie, Phys. Rev. B **38**, 1148 (1988).

[27]M. A. Ruderman and C. Kittel, Phys. Rev. **96**, 99 (1954).

[28]S. Fraga, *Handbook of Atomic Data* (Elsevier, New York, 1976).

[29]N. Bloembergen, E. M. Purcell, and R. V. Pound, Phys. Rev. **73**, 679 (1948).

[30]E. L. Hahn, Phys. Rev. **80**, 580 (1950).

[31]H. Y. Carr and E. M. Purcell, Phys. Rev. B **94**, 630 (1954); S. Meiboom and D. Gill, Rev. Sci. Instrum. **29**, 688 (1958).

[32]G. Grüner, A. Zawadowski, and P. M. Chaikin, Phys. Rev. Lett. **46**, 511 (1981).

[33]G. Grüner *et al.*, Phys. Rev. Lett. **45**, 935 (1980).

[34]J. Dumas and D. Feinberg, Europhys. Lett. **2**, 555 (1986).

[35]H. Matsukawa and H. Takayama, Physica **143B**, 80 (1986).